Decadal Variability of the ENSO Teleconnection to the High-Latitude South Pacific Governed by Coupling with the Southern Annular Mode*

RYAN L. FOGT AND DAVID H. BROMWICH

Polar Meteorology Group, Byrd Polar Research Center, and Atmospheric Sciences Program, Department of Geography, The Ohio State University, Columbus, Ohio

(Manuscript received 29 June 2004, in final form 10 August 2005)

ABSTRACT

Decadal variability of the El Niño–Southern Oscillation (ENSO) teleconnection to the high-latitude South Pacific is examined by correlating the European Centre for Medium-Range Weather Forecasts (ECMWF) 40-yr Re-Analysis (ERA-40) and observations with the Southern Oscillation index (SOI) over the last two decades. There is a distinct annual contrast between the 1980s and the 1990s, with the strong teleconnection in the 1990s being explained by an enhanced response during austral spring. Geopotential height anomaly composites constructed during the peak ENSO seasons also demonstrate the decadal variability.

Empirical orthogonal function (EOF) analysis reveals that the 1980s September–November (SON) teleconnection is weak due to the interference between the Pacific–South American (PSA) pattern associated with ENSO and the Southern Annular Mode (SAM). An in-phase relationship between these two modes during SON in the 1990s amplifies the height and pressure anomalies in the South Pacific, producing the strong teleconnections seen in the correlation and composite analyses. The in-phase relationship between the tropical and high-latitude forcing also exists in December–February (DJF) during the 1980s and 1990s.

These results suggest that natural climate variability plays an important role in the variability of SAM, in agreement with a growing body of literature. Additionally, the significantly positive correlation between ENSO and SAM only during times of strong teleconnection suggests that both the Tropics and the high latitudes need to work together in order for ENSO to strongly influence Antarctic climate.

1. Introduction

The Tropics are an area of high variability on interannual and interdecadal time scales. Periods of active convection or extreme drought associated with tropical oscillations can have adverse effects on local climates, such as flooding in western South America or wildfires in Australia (e.g., Bell et al. 2000; Bell and Halpert 1998). El Niño–Southern Oscillation (ENSO), which is associated with the cycle of warm and cold sea surface temperature (SST) anomalies in the central and eastern equatorial Pacific, has impacts that affect global climate on interannual and interdecadal time scales (e.g., Karoly et al. 1996). One area where the ENSO teleconnection appears particularly strong in the high southern latitudes is in the South Pacific Ocean, off the coast of Antarctica and in the vicinity of the Drake Passage (see Turner 2004 for a review).

In the southeast Pacific, a large blocking high pressure forms as a response during El Niño, that is, an ENSO warm event (Renwick and Revell 1999; Renwick 1998; van Loon and Shea 1987). The low-frequency variability is readily seen in the amplitude of this pressure center, which is part of the Pacific–South American (PSA) pattern (Mo and Ghil 1987). Similar to its counterpart in the Northern Hemisphere, the Pacific–North American (PNA) pattern (Wallace and Gutzler 1981), the PSA represents a series of alternating positive and negative geopotential height anomalies extending from the west-central equatorial Pacific through Australia–New Zealand, to the South Pacific near Antarctica–South America, and then bending northward toward Africa. This pattern follows a great circle trajectory, and has been shown to be induced by

* Byrd Polar Research Center Contribution Number 1315.

Corresponding author address: Ryan L. Fogt, Polar Meteorology Group, Byrd Polar Research Center, The Ohio State University, 1090 Carmack Rd., Columbus, OH 43210.
E-mail: rfogt@polarmet1.mps.ohio-state.edu

upper-level divergence initiated from tropical convection (Revell et al. 2001), and is thus related to ENSO.

There is a need to better understand the decadal variability of the ENSO signal in high southern latitudes. Results from Cullather et al. (1996) and Bromwich et al. (2000) indicate a strong shift in the correlation between West Antarctic (180°–120°W) precipitation minus evaporation ($P - E$) and the Southern Oscillation index (SOI) using atmospheric reanalysis and operational analysis over the last two decades. The time series of $P - E$ was positively correlated with the SOI until about 1990, after which it became strongly anticorrelated, a relationship that persisted through at least 2000. Furthermore, Genthon et al. (2003) and Genthon and Cosme (2003) note variability in the correlation between the SOI and the 500-hPa geopotential height field in the southeast Pacific from the 1980s and the 1990s using reanalysis and model output. However, Genthon and Cosme (2003) disagree with Bromwich et al. (2000) regarding the switch of the correlation sign between $P - E$ and the SOI from the 1980s to the 1990s, suggesting that the correlation is continually negative, albeit weakly during the 1980s. Regardless, both studies agree on the distinct changes between the 1980s and the 1990s. Recently, Bromwich et al. (2004) identified significant shifts in the position of convection and the associated amplification of the PSA wave train in December–February (DJF) in the late 1990s El Niño − La Niña difference versus the difference between all other El Niños and La Niñas from 1979 to 2000. Thus, there appears to be strong decadal variability of the ENSO signal in the South Pacific; however, the mechanisms forcing the variability remain undetermined.

In trying to understand these mechanisms, more knowledge is needed on the variability of the Southern Hemisphere circulation. In the high southern latitudes, the dominant mode of the circulation variability is the high-latitude mode, which has also been referred to as both the Antarctic Oscillation (AAO) and the Southern Annular Mode (SAM) (Thompson and Wallace 2000; Gong and Wang 1999). Represented as the first empirical orthogonal function (EOF) in the month-to-month 500-hPa geopotential heights (i.e., Rogers and van Loon 1982; Kiladis and Mo 1998) as well as SLP (Rogers and van Loon 1982; Gong and Wang 1999), the SAM is characterized by zonal pressure anomalies in the midlatitudes having the opposite sign of the zonal pressure anomalies over Antarctica and the high southern latitudes.

This study examines the ENSO teleconnection to the South Pacific–Drake Passage region on decadal time scales in an attempt to determine the mechanisms leading to the low-frequency variability. Section 2 describes the data and methodology used in the study. The decadal variability of the ENSO teleconnection is examined in section 3 using both reanalysis data and observations. Section 4 details the mechanisms responsible for the decadal variability seen in section 3. A discussion is presented in section 5, and a summary is offered in section 6.

2. Data and methods

Atmospheric data are provided by the European Centre for Medium-Range Weather Forecasts 40-yr Re-Analysis (ERA-40), including the monthly mean 500-hPa geopotential heights and mean sea level pressure (MSLP). Data from the 2.5° × 2.5° latitude–longitude grid were used for the time period from 1979 to 2001, and were obtained from the ECMWF Web site (available online at http://data.ecmwf.int/data/). ERA-40 has been proven to have many shortcomings in high southern latitudes (Bromwich and Fogt 2004; Sterl 2004) that limit its applicability before 1979. ERA-40 is chosen here due to its superior performance in the modern satellite era over the National Centers for Environmental Predication–National Center for Atmospheric Research (NCEP–NCAR) reanalysis (Bromwich and Fogt 2004); however, the NCEP–NCAR reanalysis provides similar conclusions and is used occasionally to independently validate the ERA-40 results.

Monthly mean MSLP observations at 28 stations poleward of 30°S are also used to confirm the quality and accuracy of ERA-40. MSLP observations for Antarctica were obtained from the British Antarctic Survey READER project Web site (available online at http://www.antarctica.ac.uk/met/READER/). The MSLP data for the remaining stations were obtained until 1998 through the NCAR ds570.0 dataset, with the recent years completed from data available through the National Climatic Data Center (NCDC; http://www.ncdc.noaa.gov/oa/ncdc.html).

The SOI was calculated using the monthly mean sea level pressure differences between Tahiti (17.5°S, 149.6°W) and Darwin, Australia (12.4°S, 130.9°E), obtained from the Climate Prediction Center (CPC, see online at http://www.cpc.noaa.gov). To be consistent with our analysis, the SOI was standardized over the 1979–2001 interval. An index for the SAM was calculated based on the definition of Gong and Wang (1999), using the difference between the standardized zonal monthly sea level pressure anomalies from ERA-40 at 40° and 65°S. As with the SOI, these anomalies were standardized over the 1979–2001 interval. A positive

SAM index indicates lower (higher) pressures over Antarctica (midlatitudes).

Annual means, averaged from May to the following April (Trenberth and Caron 2000), are used to remove the seasonal cycle and to capture the evolution of an ENSO event, which generally peaks during September through February. However, the seasonal cycle is often important when considering the effects of ENSO and is calculated based on the traditional seasons of austral spring [September–November (SON)], austral summer (DJF), austral fall [March–May (MAM)], and austral winter [June–August (JJA)]. Seasonal means are used, where the three months are averaged together to represent the respective season, unless otherwise stated.

Spatial correlation analysis is used to demonstrate the ENSO teleconnections across the Southern Hemisphere. Significance levels of the correlation values were determined using a two-tailed Student's t test, with eight degrees of freedom per decade since the annual and seasonal mean time series do not show any autocorrelation and are thus assumed independent. With eight degrees of freedom, correlations >0.76, >0.63, and >0.55 are significant at the 99%, 95%, and 90% confidence levels, respectively.

EOF analysis was employed using seasonal anomalies of the ERA-40 500-hPa geopotential height fields from 1979 to 2001. Seasonal anomalies, defined as the individual seasonal average minus the seasonal grand mean for the 23 years, were interpolated to a 31×31 Cartesian grid centered over the South Pole with a spacing of 450 km. Thus, the domain has edges at about 12.5°S at the corners and around 30°S at the midpoints of each side. Principal components (PCs) were constructed using the covariance matrix, and Varimax rotation was performed on the EOFs and used throughout the analysis; rotation of EOFs is encouraged (Richman 1986; Trenberth et al. 2005). For the seasonal EOFs, four factors were retained for the Varimax rotation. Four factors were chosen since the first four modes explained over 60% of the total variance and the scree plot (not shown) becomes fairly linear after the fifth eigenvalue. Retaining more factors does not significantly influence the variability in each principal component time series; only small changes result in the amount of explained variance for each loading pattern when retaining more factors.

3. Decadal variability of the ENSO teleconnection

a. Reanalysis depictions

First, the spatial correlations between ERA-40 MSLP and the SOI at each grid point in the $2.5° \times 2.5°$ reanalysis domain south of 30°S were constructed using annual means as defined earlier, as in Guo et al. (2004). The correlations were calculated using calendar decades (e.g., the 1980s represent the 10 annual means from 1980 to 1989). Bromwich et al. (2000) and Genthon et al. (2003), who demonstrated that the Antarctic ENSO variability operates on calendar decades, verify the use of them in the current study. Also presented on these plots are the correlations determined from MSLP observations at 28 stations south of 30°S. Results using the ERA-40 MSLP are given in Fig. 1 for the two decades; similar findings are observed using the NCEP–NCAR reanalysis (not shown).

In the 1980s (Fig. 1a), the teleconnection appears in the South Pacific in a band centered on 60°S, significant at >95% level. The pattern produced by ERA-40 agrees well with the observations, giving confidence that this center is robust. During the 1990s, a marked change occurs from the 1980s, with correlations now highly significant (>99% level) across nearly the entire Amundsen–Bellingshausen Seas and over the Antarctic Peninsula (Fig. 1b). The pattern again aligns well with the observations, indicated by the correlations surrounding the Drake Passage region, namely, at Faraday, Halley, Orcadas, and Punta Arenas (see Fig. 2 for a location map of the South Pacific–Drake Passage region). It becomes clear from Fig. 1 that a marked variability is operating on near-calendar decades, similar to Genthon et al. (2003) who observed the decadal variability in the 500-hPa geopotential height fields. The similarities between the surface and the midtroposphere are due to the equivalent barotropic nature of the high southern latitudes.

To view the seasonal cycle, seasonal correlations are performed using the ERA-40 500-hPa geopotential heights. Through the four seasons the correlation values change substantially and the annual mean plots are best explained by the SON (Fig. 3) and DJF (Fig. 4) correlations, the peak seasons of ENSO. During MAM and JJA (not shown), essentially no significant correlation exists during either decade. Thus, the discussion of decadal variability seen in the annual mean plots largely pertains to the variability noted in the SON and DJF patterns.

The SON plot (Fig. 3) is consistent with Fig. 1, showing substantial variability between the decades. The teleconnection in the 1980s (Fig. 3a) is weak and more zonally elongated than the 1990s, suggesting a disruption in the circulation or in the propagation of the tropical signal to the high southern latitudes during austral spring. Notably, the 1990s demonstrate a statistically significant (>99% level) teleconnection across a much larger region in the South Pacific compared to the 1980s.

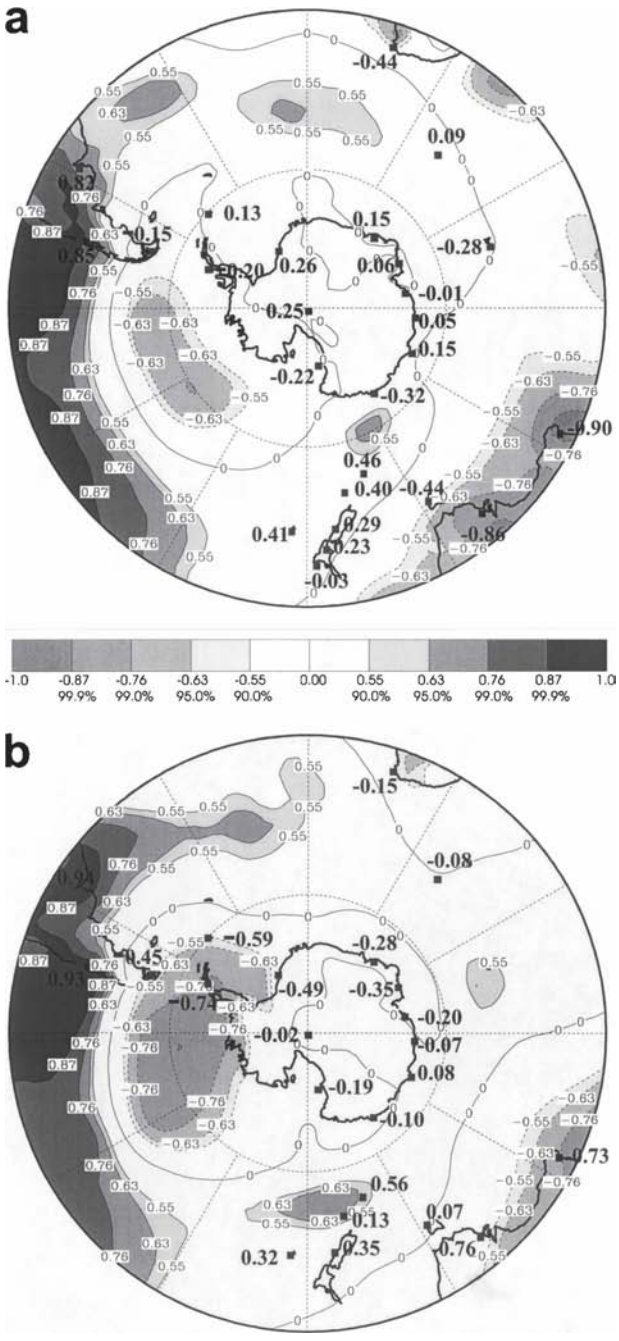

FIG. 1. Spatial correlations of ERA-40 MSLP and the SOI for the (a) 1980s and (b)1990s. Also plotted are the observed MSLP–SOI correlations for select stations south of 30°S; at the South Pole station surface pressure was used instead of MSLP. Significance levels for correlation values are listed under the key.

The DJF plots produce quite a different picture in terms of the variability between the decades (Fig. 4). Instead of the large differences between the 1980s and 1990s as seen in the annual mean and SON plots, the 1980s and 1990s are quite similar, both maintaining a strong teleconnection to the South Pacific although with a different spatial representation: the teleconnection maximum is located near 60°S, 135°W during the 1980s (Fig. 4a) but shifts both south and east in the 1990s, placing the maximum along the Bellingshausen Sea–Antarctic Peninsula coastline (Fig. 4b).

Through examination of the seasonal correlation plots, the variability presented in the annual mean plots (Fig. 1) is better understood. Although there are differences between the 1980s and the 1990s DJF patterns, the correlations in the majority of the South Pacific are significant at >95% level and only the spatial pattern is changed. In SON, large changes occur between the 1980s and the 1990s, from essentially no significant correlation in the 1980s to a large area across the South Pacific significant at >99% level in the 1990s. Thus, the differences noted between the annual mean patterns for the 1980s and the 1990s can primarily be explained by the substantial differences in SON between the two decades.

b. ENSO composites for SON and DJF

When looking at ENSO variability in the South Pacific, many previous studies have used composite techniques based on the tropical Pacific SSTs (e.g., Karoly 1989; Harangozo 2000; Turner 2004). However, these studies have only examined the ENSO teleconnection during austral winter, when no significant correlation is found in either decade. Thus, it is not surprising that previous studies have not described the decadal variability of the ENSO teleconnection. It has only appeared in studies that used annual means (e.g., Bromwich et al. 2000; Genthon et al. 2003), thus capturing the significant teleconnections during austral spring and austral summer, as described earlier. Kwok and Comiso (2002) also constructed ENSO composites based on the sign of the SOI from 1982 to 1998 and found seasonal variability in the anomaly signal in the South Pacific. However, their study does not find the decadal variability in these composites, despite breaking the time interval into two 8-yr periods. Kwok and Comiso do not explicitly examine the seasonality in these two 8-yr periods, and this could explain why they did not observe decadal variability in their composites.

Notably, ENSO composites (El Niño minus La Niña) for SON and DJF do resemble the decadal variability seen in the correlation plots (Fig. 5). There were three warm events during SON and DJF in both the 1980s and 1990s; during these two seasons there were also two and three cold events for the 1980s and 1990s, respectively. These events are based on the definition of Trenberth (1997) and are listed in Table 1. Trenberth's calculation used a SST threshold of 0.4°C (positive for

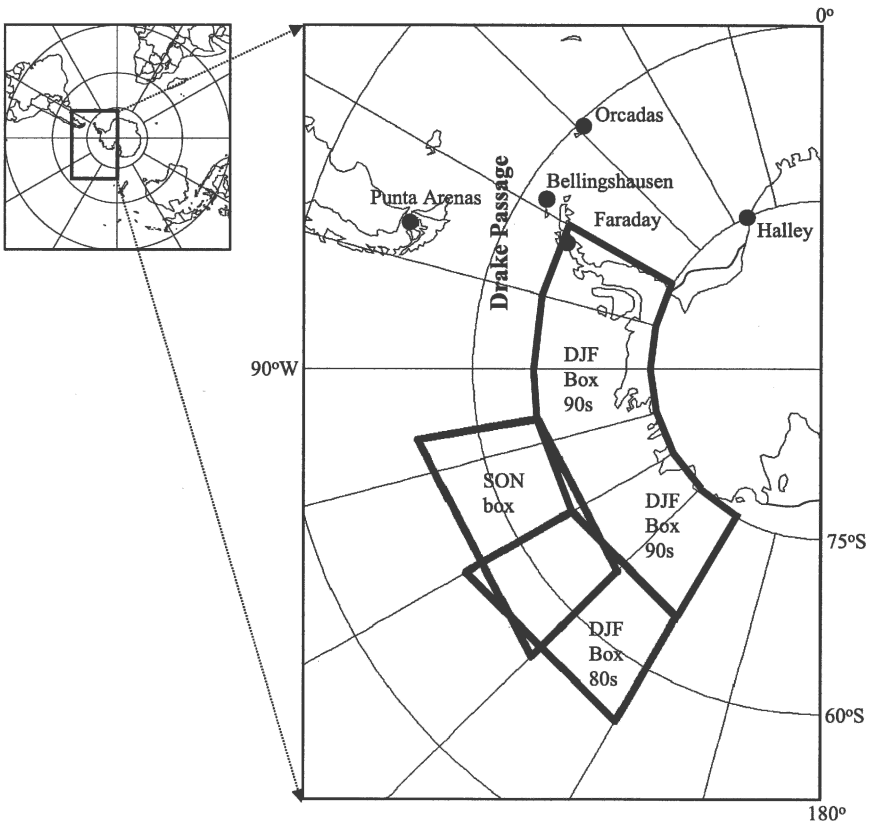

FIG. 2. Locations of stations and box regions in the South Pacific as referenced in the text.

warm El Niño events, negative for cold La Niña events) from a 5-month running mean of the SST anomalies in the Niño-3.4 region (5°N–5°S, 120°–170°W). To be considered an event, the threshold must persist for six months. Additionally, Trenberth (1997) cautions on the use of the unsmoothed SOI to construct seasonal ENSO composites, noting that many high-frequency phenomena (including the Madden–Julian oscillation) can influence an unsmoothed SOI time series, and not represent variability within the Southern Oscillation itself.

The negative correlation contours in the South Pacific in Figs. 3 and 4 indicate higher pressures/heights in these regions during El Niño events (SOI < 0), while the composites (Fig. 5) indicate that heights in the South Pacific are significantly higher during El Niño events than they are during La Niña events (shading represents the $>95\%$ confidence level tested against the null hypothesis that the difference between El Niño and La Niña events is zero). Thus, the composites constructed for each season and decade reproduce the decadal variability seen in the preceding correlation plots. Previous studies, such as Turner (2004), miss the decadal variability by both averaging over a longer period and not considering the austral spring or summer teleconnections. Although Turner (2004) displays similar composites for austral winter as those seen above, the magnitudes of the anomaly centers are weaker and likely not statistically significant. However, the present results indicate that compositing techniques can capture the decadal variability when seasonality and shorter time intervals are considered.

c. *Observational depictions*

Decadal changes in the atmospheric circulation as a response to the large ENSO-induced variability in the South Pacific should be seen in the observations as well. The negative correlation isolines in the South Pacific in Fig. 1 can be treated as isobars. They suggest that during an El Niño event (SOI < 0) a stronger high pressure forms in this region, in agreement with previous studies (e.g., Renwick 1998; van Loon and Shea 1987). The correlation pattern also observed in the 500-hPa geopotential heights creates a southerly (off Antarctic) geostrophic wind in the vicinity of Drake Passage. Furthermore, because of the large area of positive correlations across the subtropical jet region ($\sim$30°S), the local pressure gradient is weakened, causing weaker

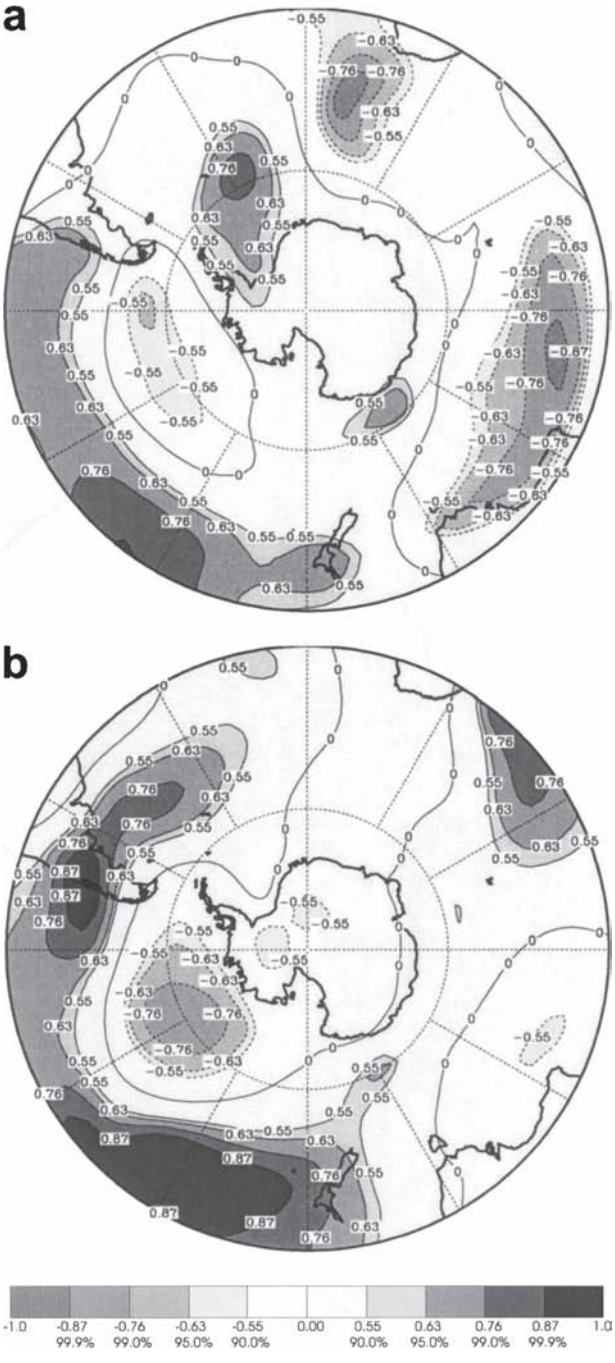

FIG. 3. ERA-40 SON 500-hPa geopotential height correlations with the SOI for the (a) 1980s and (b) 1990s. Significance levels are listed below the key.

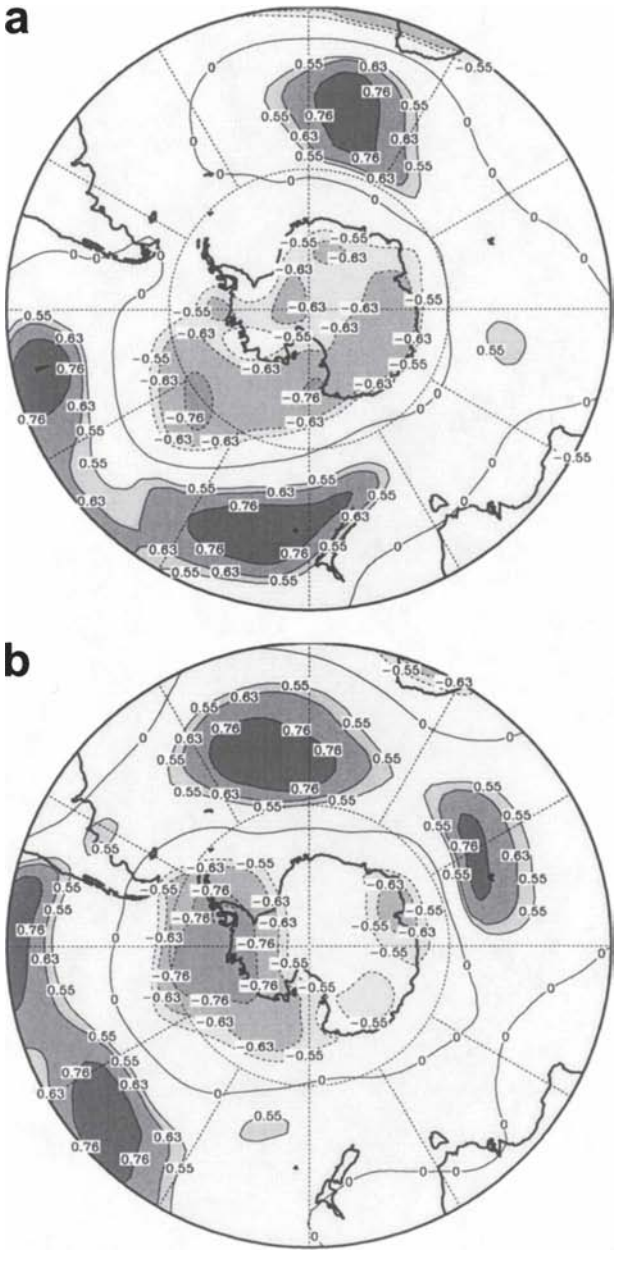

FIG. 4. As in Fig. 3 but for DJF; see key in Fig. 3.

westerly winds during El Niño conditions (SOI < 0) across southern South America. More southerly (positive v) and easterly (negative u) winds during an El Niño event, when the SOI is negative, suggest a negative correlation with the meridional wind over the Antarctic Peninsula and a positive correlation with the zonal wind over southern South America.

Upper-air observations from Bellingshausen, on the Antarctic Peninsula, and Punta Arenas, Chile (Fig. 2), verify the upper-level meridional and zonal wind correlations described above and are displayed in Fig. 6 for the 1980s and the 1990s, the period of available data. The 500-hPa winds were chosen over surface winds so that the complex topography at both Punta Arenas and Bellingshausen would not significantly affect the results. The missing daily values in the radiosonde records were estimated by bilinearly interpolating the ERA-40 values to the station locations; however, this

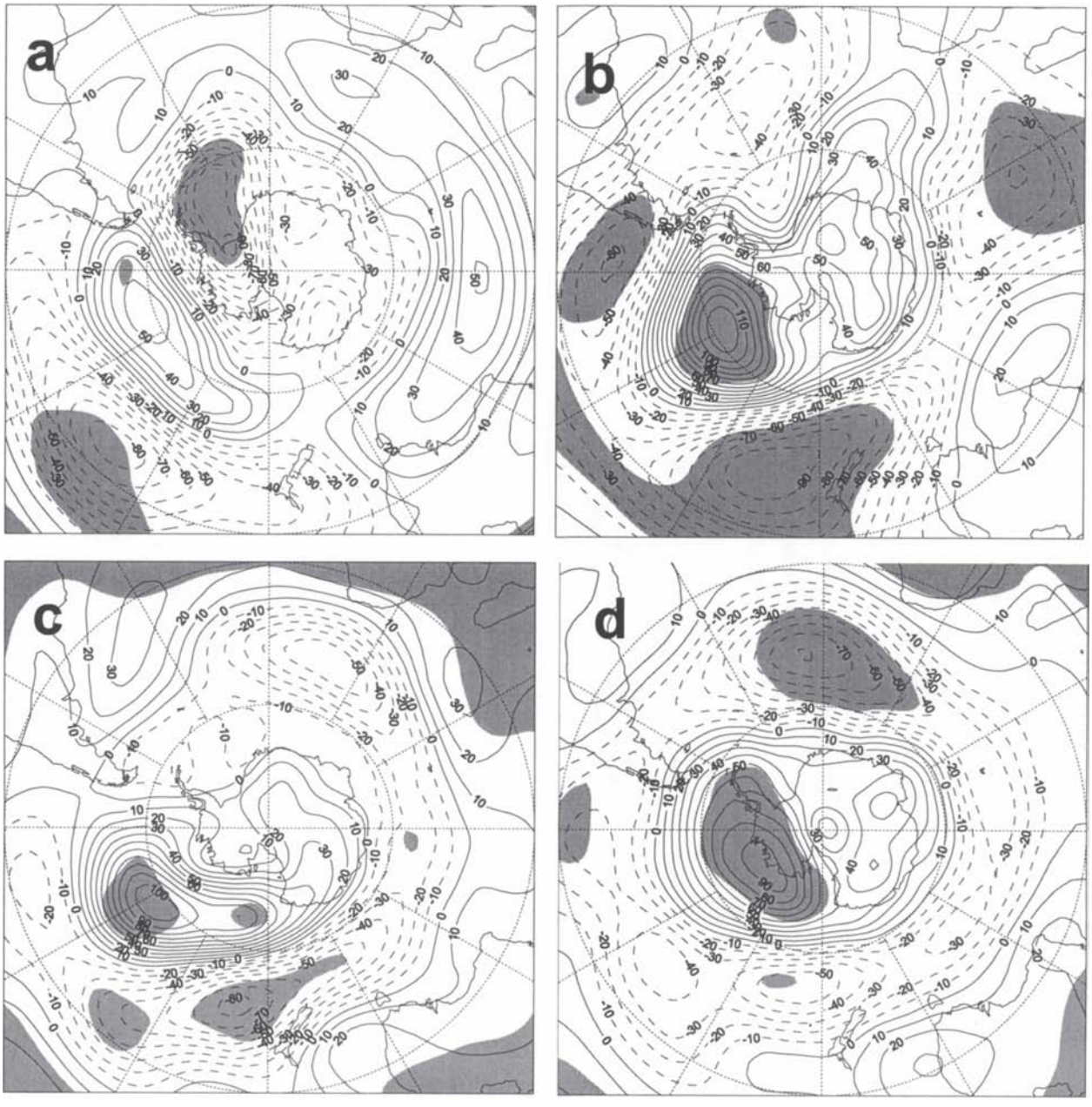

FIG. 5. ERA-40 500-hPa geopotential height anomaly ENSO composites (El Niño minus La Niña) for the events listed in Table 1: (a) SON 1980s, (b) SON 1990s, (c) DJF 1980s, and (d) DJF 1990s. Contour interval is 10 gpm, shaded regions denote differences significant at >95% confidence level.

interpolation does not affect the results on the annual time scales shown here. In Fig. 6b, ERA-40 meridional winds were used to extend the radiosonde record in order to capture the El Niño event of 1997–98; radiosonde data for Bellingshausen were unavailable after 1996.

In the 1980s there is a marginally significant correlation of the SOI and ERA-40 MSLP west of the Drake Passage region (Fig. 1a). As a result, this should reduce correlations of upper-level winds at these two locations with the SOI. This is seen in Fig. 6, as the correlations during the 1980s are well below significant levels.

During the 1990s when the strong negative correlations of the SOI and ERA-40 MSLP arise across much of the South Pacific (Fig. 1b), a pronounced reflection becomes evident in the upper-air observations in Fig. 6 as the correlations with the SOI are now statistically significant at >99% level. Thus, the observations also

TABLE 1. SON and DJF ENSO events (1980–99) following Trenberth (1997). DJF events are defined from the December of each year.

Year	Type
1982	Warm
1984	Cold
1986	Warm
1987	Warm
1988	Cold
1991	Warm
1994	Warm
1995	Cold
1997	Warm
1998	Cold
1999	Cold

verify the strong decadal variability from the 1980s to the 1990s, set up by the implied modulation of the local pressure gradients in the 1990s by ENSO. The decadal changes are especially large and statistically significant at >99% confidence level at Punta Arenas.

4. Mechanisms leading to decadal variability

A previous study by Mo and Higgins (1998) shows the linkage between the tropical convection and the PSA modes. They identify two PSA modes in the SH winter, PSA1 and PSA2, using the NCEP–NCAR and the NASA Data Assimilation Office reanalyses. The PSA1 mode is associated with enhanced convection in the Pacific between 140°E and 170°W and suppressed convection over the Indian Ocean. Spatially, their PSA1 mode appears as a large center in the South Pacific Ocean. The PSA2 mode is forced by positive convective anomalies in the central Pacific from 160°E to 150°W just south of the equator and suppressed convection over the western Pacific and appears as a wave-3 pattern in the high southern latitudes. Mo and Peagle (2001) later infer that the PSA1 mode is linked with the interannual component of ENSO, positive during El Niño events and negative during La Niña events. They also find that the PSA2 mode has ties to the quasi-biennial (22–28 months) component of ENSO, again positive during El Niño events and negative during La Niña events. The PSA mode associated with each ENSO event is largely governed by the position of the tropical convection.

Turner (2004) provides a contemporary summary regarding the dynamics of the ENSO signal transmission to higher latitudes, detailing that this tropical signal is transported to the high southern latitudes via the PSA. He shows that there is much variability in this transmission (e.g., Houseago et al. 1998), but does not provide a definitive explanation leading to the variability between the PSA and the magnitude of the ENSO teleconnection. Turner (2004) also suggests a need for more research on the linkage between the SAM (the dominant circulation pattern in the high southern latitudes) and Antarctic climate. It is likely that the decadal variability in the ENSO teleconnection is coupled with the variability of the SAM, especially in light of the findings of Mo (2000) who relates the SAM to tropical convection.

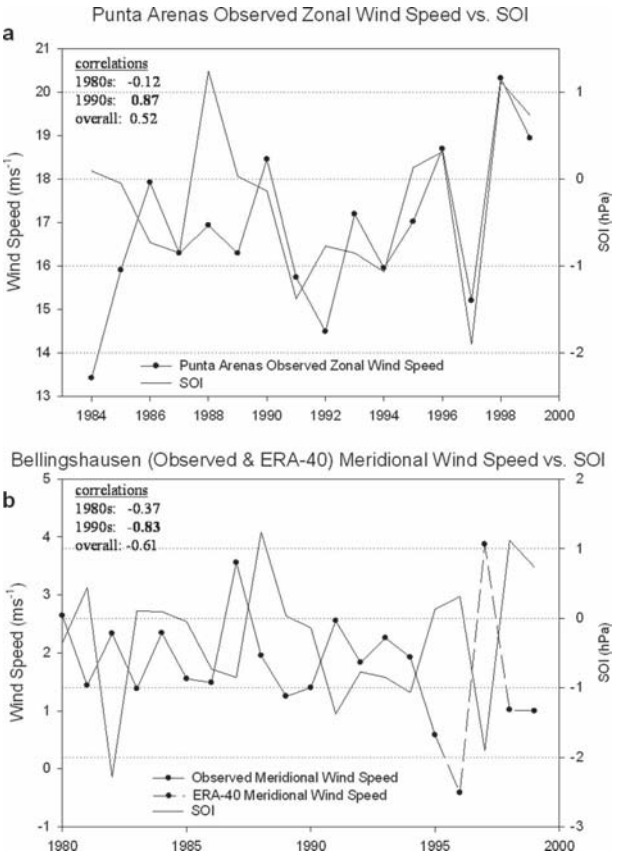

FIG. 6. Annual mean time series of (a) observed 500-hPa zonal wind at Punta Arenas, Chile, vs SOI and (b) observed (solid line) and ERA-40 (dashed line) 500-hPa meridional wind speed at Bellingshausen, Antarctica, vs SOI. ERA-40 meridional winds were used in (b) so that the record is extended to capture the pronounced El Niño and La Niña events in the late 1990s. Correlations are listed in the upper-left-hand corner for each figure; the boldface correlations in the 1990s are significant at >99% level.

a. SON ENSO and SAM interactions

By averaging the 500-hPa geopotential heights in a South Pacific region (55°–65°S, 135°–100°W; labeled "SON box" in Fig. 2) for SON, a time series representing the ENSO teleconnection is generated. This region

was chosen as it represents the area of the maximum correlation seen in the SON seasonal mean plot during the 1980s and 1990s (Fig. 3). Looking at this time series for SON versus the austral spring SOI (Fig. 7a), the low correlations in the 1980s and the strong anticorrelation in the 1990s can be identified. However, there is a significant positive height anomaly during the 1982 El Niño, yet interestingly no significant negative height anomaly response during the 1988 La Niña. Furthermore, in the 1990s there is a phase-locked response with the SOI and the height anomalies where the height fields respond to nearly all of the small changes in the SOI; the strong anticorrelation persists until the year 2000. The seasonal means used here effectively include the lag time for the atmosphere to respond to the forcing in the Tropics, which operates on time scales of less than a month (Thompson and Lorenz 2004; Mo and Peagle 2001).

To examine the phase locking between the SOI and the height anomalies in the South Pacific during SON in terms of the circulation variance, EOF analysis is performed using the SON seasonal anomalies throughout the time period. EOF results obtained using monthly anomalies (not shown) are representative of previous results (e.g., Kiladis and Mo 1998; Mo 2000), giving confidence to the results displayed here using seasonal anomalies.

The rotated EOF (REOF) patterns constructed from the ERA-40 reanalysis are presented in Fig. 8. After rotation, in SON the SAM pattern appears as the first mode, explaining 24.9% of the variance. The PSA1 mode appears next with 17.8% of the variance and the PSA2 mode appears third with 13.4% of the variance. The fourth pattern is a wave-3 pattern in the high southern latitudes that is not related to either SAM or ENSO activity. Correlations of the ERA-40 RPCs with the SOI and SAM are listed in Table 2.

REOF results conducted using the NCEP–NCAR reanalysis are very similar (Fig. 9), except that the PSA1 mode dominates with 21.7% of the variance and the SAM is second with 20.2%. However, these two modes explain very similar proportions of the total variance and are thus not separable (North et al. 1982). The third and fourth ranked REOF patterns represent wave-3 modes and appear in a different order in terms of explained variance than in ERA-40. The third pattern from the NCEP–NCAR also correlates with the SAM, due to its general structure in which anomalies of one sign reside in the high latitudes, and anomalies of the opposite sign reside in the middle latitudes (except the South Pacific). Despite the slight changes in variance, the rotated principal component (RPC) time series are very similar for ERA-40 and NCEP–NCAR, especially in terms of the PSA1 mode. Thus, both ERA-40 and NCEP–NCAR capture the high southern latitude ENSO variability quite well, and the NCEP–NCAR results stand to validate those of ERA-40 for this time period.

Although of different sign (which are arbitrary in EOF patterns) and position, it is noteworthy that both PSA modes and SAM all have large loading centers in the South Pacific and Amundsen–Bellingshausen Seas region. The spatial overlap of these loading centers indicates that both ENSO and the SAM significantly influence the 500-hPa geopotential height variance in this region. Notably, the overlap occurs in the location of highest correlation seen in the SON plot during the 1990s (Fig. 3b). This finding was seen earlier in the 500-hPa time series extracted from the 55°–65°S, 135°–100°W box, where the 500-hPa height anomalies during the 1990s responded strongly to the variability in the SOI (Fig. 7a). It can be seen that the height fields also respond to changes in the SAM in the 1990s (Fig. 7b). In the 1980s, the 500-hPa height anomalies in this region respond to nearly every oscillation in the SAM, yet the ENSO teleconnection in this decade and season is not significant because the coupling with ENSO is absent. Figure 7c displays the coupling between the SOI and the SAM; the two oscillations are significantly correlated (0.71) only in the 1990s. This finding is in agreement with Silvestri and Vera (2003), who find significant correlation in the austral spring SAM and ENSO over the 1979–99 time period, despite the fact that their study overlooked the decadal variability in the ENSO–SAM relationship. Additionally, the decadal variability in the SAM–SOI correlation can be seen in other SAM indices, such as the SON RPC1 time series (Table 2).

During the 1988 La Niña in SON, the SAM and the SOI have opposing signs (Fig. 7c), indicating that these oscillations are out of phase. Harangozo (2000) describes the coupling between the zonal circulation and the ENSO teleconnection in the South Pacific, noting that westerlies in the central South Pacific are modulated by Rossby wave activity. The lack of coupling between the SAM and ENSO in the 1980s indicates that the Rossby waves did not modify the westerly wind, thereby disrupting the transport of the signal during this period. In turn, no marked anomaly response is produced in this decade (Fig. 7a). It is the combination of both mechanisms working in phase that leads to the strong ENSO teleconnection in the South Pacific.

The composites for SON (Figs. 5a and 5b) also show that the coupling between ENSO and the SAM amplify the response in the South Pacific. The 1980s composite

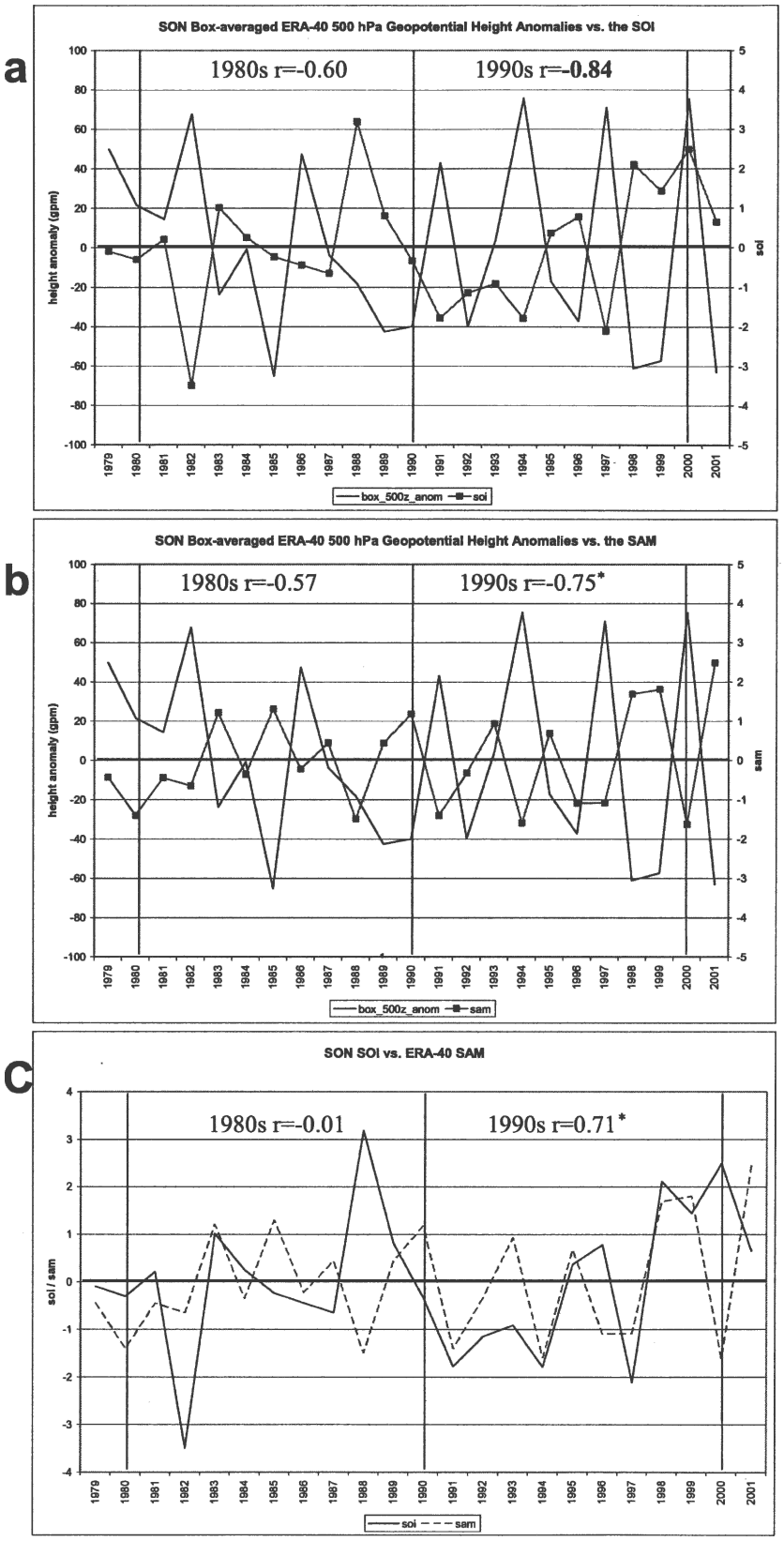

FIG. 7. ERA-40 500-hPa geopotential height anomalies averaged in a box (55°–65°S, 135°–100°W) 1979–2001 SON plotted with the SON average: (a) SOI, (b) SAM, (c)SON SOI vs SON SAM. Asterisks denote correlations significant at >95% level; boldface correlations significant at >99% level.

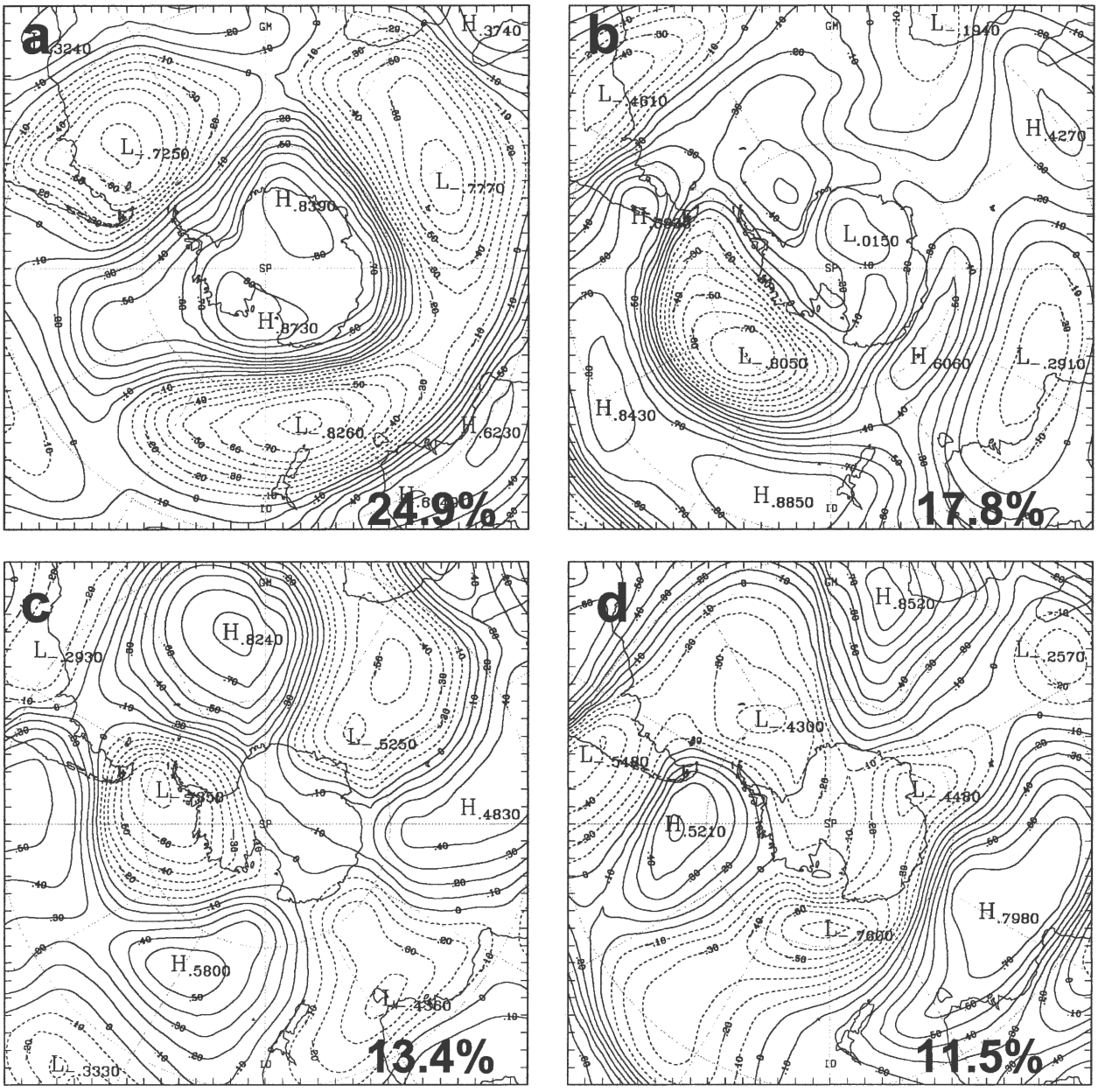

FIG. 8. The first four leading Varimax-rotated EOFs of SON 500-hPa geopotential height anomalies constructed from ERA-40 for 1979–2001. Percentage of variance explained is given in the bottom-right-hand corner of each figure: (a) REOF1, (b) REOF2, (c) REOF3, and (d) REOF4. The signs of the loading centers are arbitrary.

(Fig. 5a) shows that the positive anomaly center is not statistically significant and is located near the South American coast away from the Antarctic continent. Additionally, the height anomalies over the Antarctic continent are of opposite sign to the ENSO-related height anomalies. During the 1990s (Fig. 5b), the anomaly center is amplified, now significant at >95% confidence level, and is the same sign as the height anomalies over Antarctica. The structure of the 1990s composite shows a marked similarity to the SAM pattern seen in Fig. 8a. This further demonstrates the role of the coupling between ENSO and the SAM in producing the strong teleconnection. The SAM signal is also significantly amplified in the midlatitudes in nearly all of the loading centers (cf. Figs. 5b and 8a, the SAM REOF for SON) in the 1990s, while in the 1980s (Fig. 5a) the ENSO composite does not have a zonal signature in the midlatitudes.

TABLE 2. SON and DJF ERA-40 RPC correlations with the SOI and the SAM for the 1980s and 1990s: asterisks indicate significance at >95% level; boldface at >99% level.

Time series	Decade	SON		DJF	
		SOI	SAM	SOI	SAM
RPC1	1980s	0.16	**−0.88**	0.66*	**0.86**
	1990s	−0.50	−0.75*	0.57	0.66*
RPC2	1980s	**0.79**	−0.11	0.56	0.59
	1990s	**0.83**	0.74*	0.39	0.64*
RPC3	1980s	**−0.88**	−0.12	−0.40	−0.05
	1990s	−0.16	0.35	−0.39	0.19

b. Extension to DJF

In DJF, the ENSO teleconnection appears pronounced in both the 1980s and the 1990s (Fig. 4) but shifts south and east in the South Pacific between the two decades. During the 1980s, the strongest correlations are seen around 55°–65°S, 150°–120°W, while in the 1990s the teleconnection is stronger, yet much closer to the West Antarctic coast and the Antarctic Peninsula, around 65°–75°S, 60°–150°W.

Examining the REOF patterns for this season (Fig. 10) demonstrates again that the first two modes, representing ENSO and the SAM, respectively, influence the height variance in the South Pacific, especially the REOF1 pattern. Notably, the ENSO–RPC1 pattern is significantly correlated with both the SAM and the SOI in the 1980s (Table 2), while in the 1990s the SAM is significantly correlated with both the ENSO–RPC1 pattern and the more zonally symmetric structure in SAM–RPC2. The changes in the correlations of the SAM index between the two RPC time series suggest changes in the structure of the SAM between the two decades, perhaps due to the marked strengthening of the SAM during the 1990s in DJF (Marshall 2003).

Similar to the analysis for SON, the DJF ERA-40 500-hPa geopotential height anomalies were averaged in the region 55°–65°S, 150°–120°W (labeled "DJF box 80s" in Fig. 2), the area of strongest correlation seen in the 1980s DJF (Fig. 4a). Notably, this region corresponds with the loading center in the South Pacific from the ENSO–REOF1 pattern (Fig. 10a). The anomalies from this region are plotted along with the SOI and SAM in Fig. 11a. During the 1980s, it is clear that the height anomalies respond to fluctuations in both the SOI and the SAM, giving physical meaning to the significant correlation of SAM and SOI with the RPC1 time series and suggesting that these two modes working together amplify the anomaly response. The negative correlations persist into the 1990s, but drop below the 95% significance level, as the overall pattern shifts away from this region (Fig. 4b). To account for this south and eastward shift, ERA-40 500-hPa geopotential height anomalies were averaged in the region 65°–75°S, 60°–150°W (labeled "DJF box 90s" in Fig. 2) as before and are presented in Fig. 11b. From the time series in Fig. 11b, it can be seen that the height anomalies are significantly correlated with both the SOI and the SAM in the 1990s, again supporting the finding that the region where the ENSO teleconnection in the South Pacific appears strongest is governed by coupling with the SAM forcing.

The south and east shifting seen in the DJF correlation plots (Fig. 4) and the DJF composites (Figs. 5c and 5d) from the 1980s to the 1990s is brought about not only by the aforementioned changes in the spatial representation of the SAM, but also from the interevent variability in ENSO. Changes in the SAM from the 1980s to the 1990s explain the southward shift; the REOF2 pattern (Fig. 10b) associated with the RPC2 time series confines the height anomalies closer to the Antarctic continent than the REOF1 pattern (Fig. 10a). Similarly, the eastward shift between the two decades is explained by the strong ENSO events in the late 1990s in this season, which produced an amplified PSA2 (REOF3, Fig. 10c) pattern during the austral summer season (Bromwich et al. 2004). The PSA2–REOF3 (Fig. 10c) center is located much farther east toward the Antarctic Peninsula compared to the PSA1–REOF1 (Fig. 10a) center, in agreement with Mo and Peagle (2001). Thus, the strong ENSO events in the late 1990s austral summer and the changing SAM pattern during this season shift the annual mean teleconnection (Fig. 1b) and DJF teleconnection (Fig. 4b).

The SAM–ENSO coupling is again seen in the DJF ENSO composites for both the 1980s and the 1990s (Figs. 5c and 5d). Both decades show a SAM signature; the statistically significant height anomaly in the South Pacific has the same sign as the height anomalies over the Antarctic continent, and there are zonally symmetric anomalies of the opposite sign in the midlatitudes. Notably, the 1990s (Fig. 5d) show a very strong SAM pattern with an increased area of statistical significance tightly confined to the continent, in agreement with the marked strengthening during this decade and season; this is also in agreement with the stronger correlation of the SAM with the RPC2 time series in the 1990s (Table 2).

c. Extension to previous knowledge on decadal ENSO variability, 1980–2000

The results presented here indicate that the significant correlation between ENSO and the SAM create height anomalies that amplify the ENSO response in

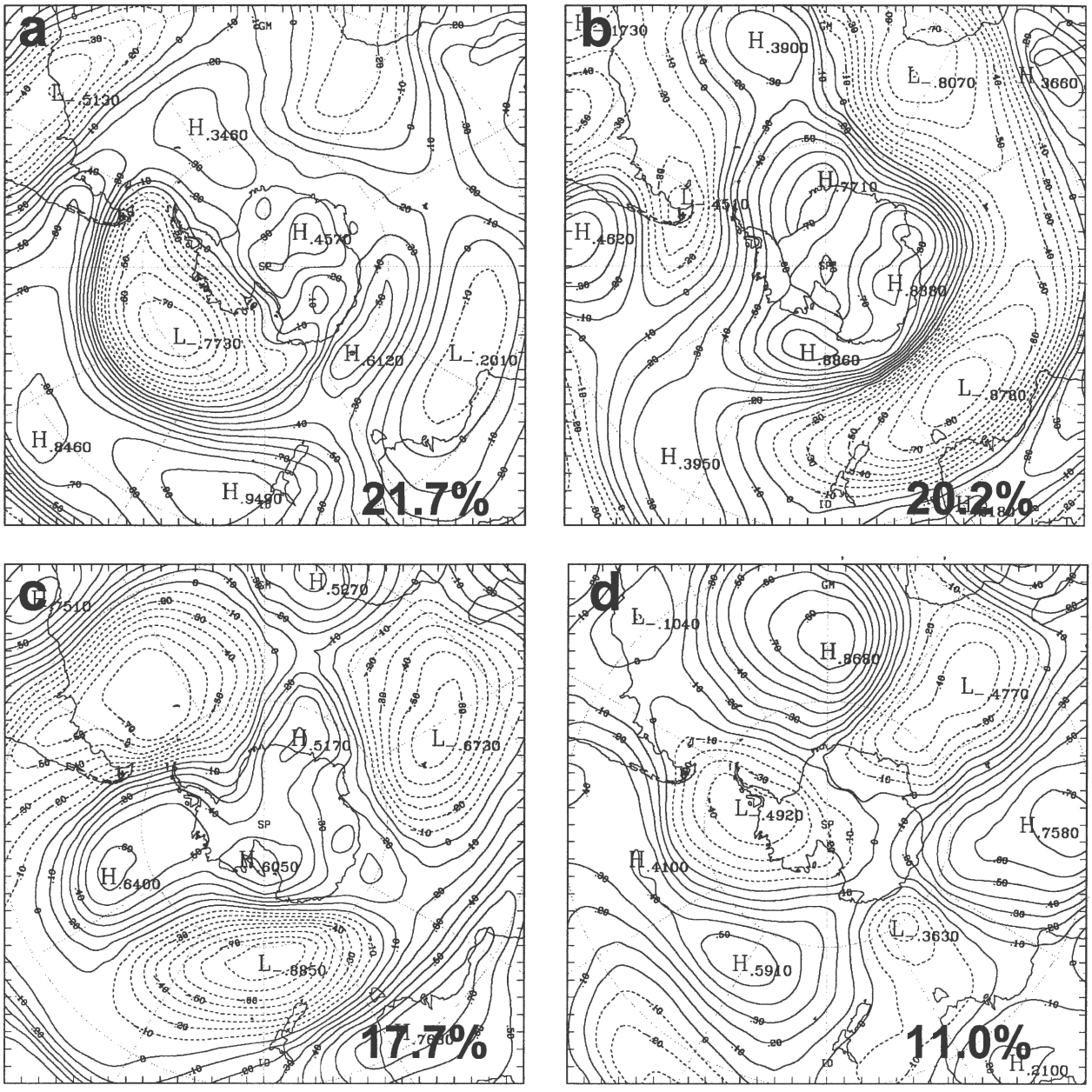

FIG. 9. As in Fig. 8 but constructed using the NCEP–NCAR reanalysis.

the South Pacific and Amundsen–Bellingshausen Seas. This finding is important as it explains much of the decadal ENSO variability with the West Antarctic precipitation minus evaporation ($P - E$) time series seen in previous studies (e.g., Cullather et al. 1996; Bromwich et al. 2000; Genthon and Cosme 2003). In light of the findings here, the persistence of a circulation anomaly during the times of strong SAM–ENSO correlation leads to an increased (decreased) moisture flux onto West Antarctica during ENSO warm (cold) events. As seen in the current study, the SAM–ENSO correlation has notable decadal changes and this, in turn, governs the large changes in the correlation between the 1980s and 1990s in the West Antarctic $P - E$ time series and the SOI.

5. Discussion

Observations (Marshall 2003) and statistical studies (Thompson et al. 2000) have displayed large trends in the SAM in austral summer and autumn, and therefore many theories have been proposed regarding the forc-

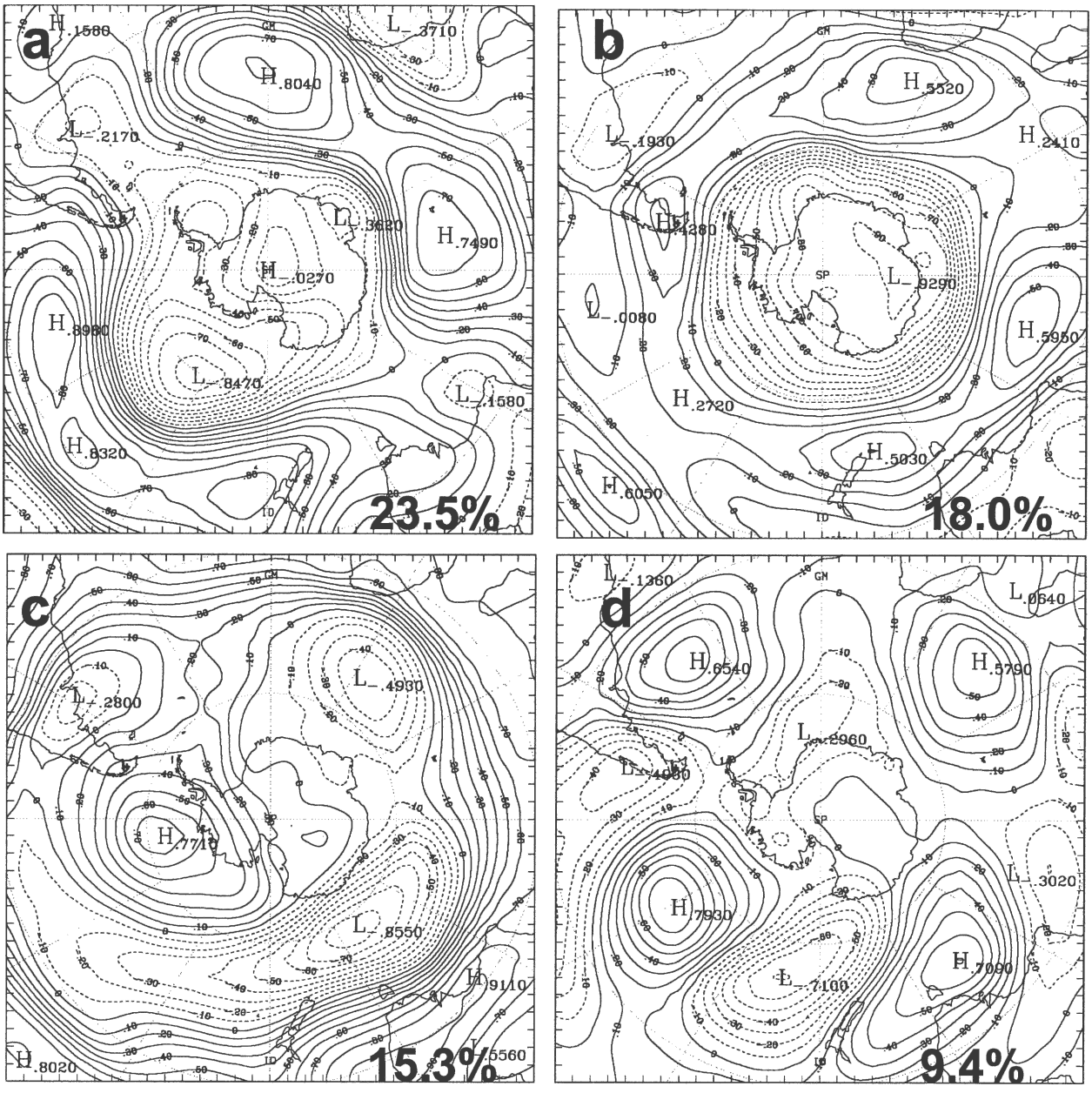

FIG. 10. As in Fig. 8 but for DJF.

ing of these trends. Thompson and Solomon (2002), using observations, suggest that in spring and summer the SAM is modulated by strong decreases in stratospheric ozone over Antarctica. Additional modeling studies by Sexton (2001) and Gillett et al. (2003) also show the linkage between ozone loss and the strengthening of the SAM.

However, Marshall (2003) finds that the tropospheric SAM lacks a trend during austral spring because tropical forcing is very strong during this season. Unlike the ozone theories, Marshall (2003) promotes the role that the Tropics play in modifying the background circulation of the Southern Hemisphere. The correlation seen here between the SAM and the SOI persisting from austral spring into austral summer further suggests that these two oscillations are not entirely independent.

Other research has questioned the role of ozone depletion in forcing the SAM. An atmosphere–ocean coupled general circulation model (GCM) study by Cai et al. (2003) demonstrated that in greenhouse warming experiments, the SAM strengthened with increasing CO_2 concentrations. Marshall et al. (2004) found

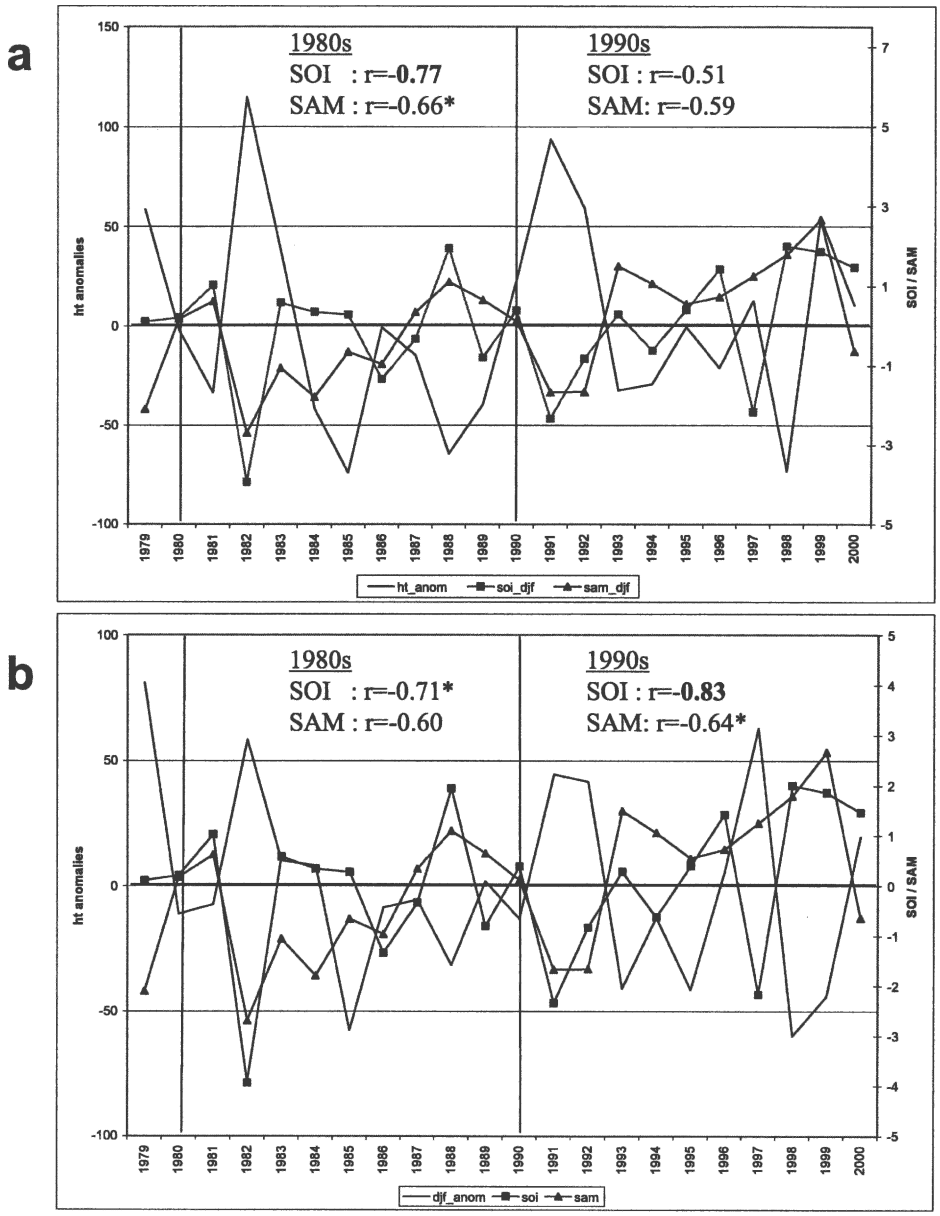

FIG. 11. DJF ERA-40 500-hPa box-averaged geopotential height anomalies averaged in the region (a) 55°–65°S, 150°–120°W and (b) 65°–75°S, 150°–60°W vs the DJF SOI and SAM. Boldface correlations are significant at >99% level; asterisks denote correlations significant at >95% level.

through a coupled GCM run that trends in the SAM begin prior to any observed decreases in the stratospheric ozone. Their study concludes that the trends result from a combination of anthropogenic forcing (by greenhouse gases) and natural climate variability. In a study by Jones and Widmann (2004), a SAM reconstruction based upon sea level pressure observations from 1905 to 2000 shows strong positive and negative trends in the middle of the record that do not match any trends in stratospheric ozone or greenhouse gases. Thus, they claim that natural forcing factors, such as solar and volcanic variability, and internal processes in the climate system can strongly influence the variability in the SAM.

There is also some support for the SAM being modulated by tropical SSTs. Mo (2000) regressed the scores from her EOF1 (which represented SAM) on SSTs and found that the SAM is linearly related to the tropical SSTs, similar to the correlation seen here between the SAM and the SOI. To examine the decadal variability

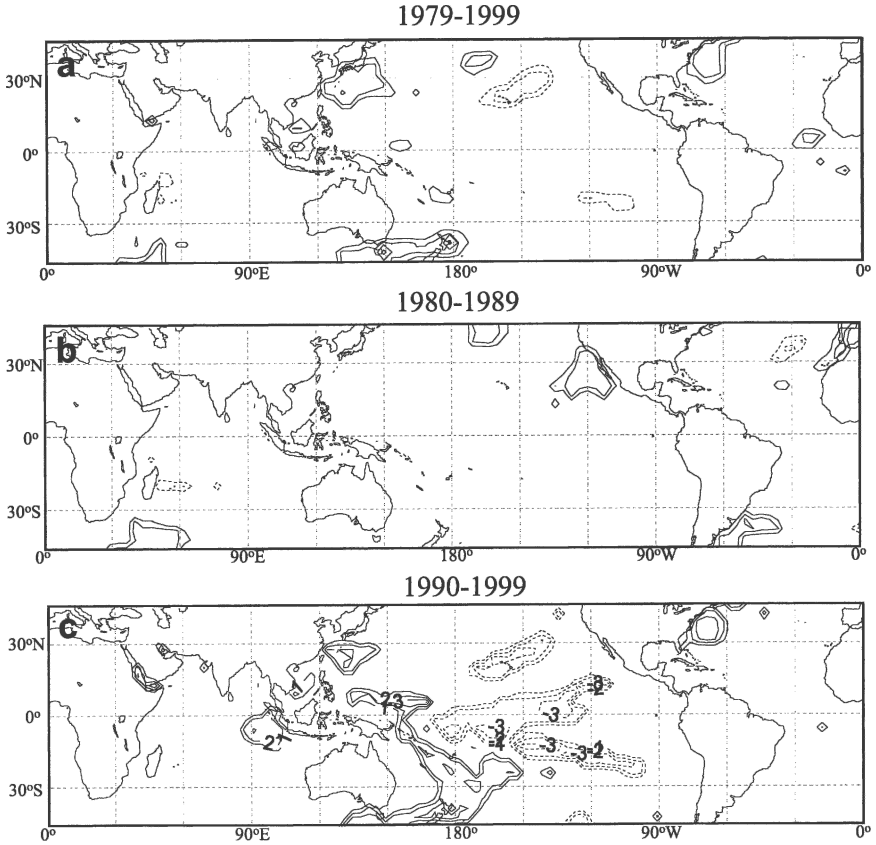

FIG. 12. SON SAM changes associated with SON SST variations from 45°S to 45°N for (a) 1979–99, (b) 1980–89, and (c) 1990–99. Contour interval is one standardized unit of the SAM; only the changes significant at >95% confidence interval are plotted. Changes are calculated by multiplying the slope of the linear regression of the SAM onto the SST anomalies by the change in SST.

in this relationship, the SON SAM was regressed onto the SON SST anomalies between 45°S and 45°N in a similar manner to Mo (2000). The regression coefficients were then multiplied by the change in SST at each grid point to represent the changes in SAM explained by the SST changes. The SST data were obtained from the National Oceanic and Atmospheric Administration (NOAA) extended reconstructed Reynold's SST dataset made available by the Climate Diagnostics Center (CDC, available online at http://www.cdc.noaa.gov/cdc/data.noaa.ersst.html). The changes significant at >95% confidence level are displayed in Fig. 12a for the whole time series and for the two decades individually (Figs. 12b,c). The overall results (Fig. 12a) do not demonstrate any large areas where changes in the SST are related to changes in the SAM, a finding that also exists during the 1980s (Fig. 12b). This is expected and verifies the fact that no significant SAM events occurred with the significant ENSO events during this decade in SON. The 1990s (Fig. 12c), however, are much different in that there is a strong and significant relationship (>95% level) between the SAM and the tropical and subtropical Pacific SST anomalies that extend into the eastern tropical Indian Ocean, unlike that seen in the previous decade. Interestingly, the changes in Fig. 12c are spatially arranged in a prominent horseshoe pattern similar to the SSTs anomalies seen during a La Niña event. Notably, during the 1990s (Fig. 12c) the southern branch of the horseshoe pattern is well marked. Terray and Dominiak (2005) relate this southern branch of the SST horseshoe pattern to the enhanced upper-level convergence brought about by the modulation of the regional meridional Hadley circulation. This upper-level convergence is associated with an upper-level low, which acts as a Rossby wave source region for the associated PSA pattern. From Fig. 12c, the negative (positive) changes in the equatorial and subtropical (western) Pacific suggests a weakening of the SAM during times of warm (cold) SSTs in this region (i.e., El Niño conditions), in agreement with the

positive correlation between the SAM and the SOI in the 1990s. Terray and Dominiak (2005) demonstrate a reduction in speed of the polar front jet in the South Pacific associated with the ENSO SST anomalies that also confirms the link between the ENSO and the SAM.

L'Heureux and Thompson (2006) also use regression analysis to examine the SAM–ENSO coupling for 1979–2004. Their study demonstrates that both oscillations are significantly related to the strength of the zonally averaged zonal wind in the high southern latitudes during austral summer. However, they do not examine the decadal variability in this relationship. An extension of their analysis (not shown) by decade reveals that the strong summer relationships seen during 1979–2004 masks the decadal variability presented in this paper. Notably, the significant relationship between ENSO and the zonally averaged zonal wind shifts from midsummer (January) during the 1980s to late fall–early summer (October–December), in agreement with the strong decadal variability of the SAM–ENSO relationship in spring and the persistence of this relationship through both decades during the summer seen here. Indeed, L'Heureux and Thompson (2006) find a significant correlation between ENSO and the SAM from 1979 to 2004 during austral summer.

Although the regression analyses do not explicitly show a cause and effect relationship of the tropical forcing on the high-latitude circulation due to the simultaneous correlation of the SOI and SAM, they do clearly demonstrate the decadal variability in this linear relationship. Partial correlation analyses do not show any connections of the SAM with the tropical Pacific SSTs; however, this statistical method only examines the linear connection with the residual variability after the cross correlation is removed. Because of the strong covariance between these two time series, the residual part of the SAM not explained by the SOI is small, and is also unlikely to depict the actual physical variability in the SAM.

Recently, a modeling study conducted using version 2 of the NCAR Community Atmosphere Model (CAM2) model confirmed the tropical SST forcing of the SAM (i.e., Zhou and Yu 2004). They also noted a significant relationship between the SAM and tropical Pacific SSTs in austral summer, where warm tropical Pacific SSTs lead to negative phases of the SAM, giving further credence to the significant positive correlation seen here between the SOI (<0 when Pacific SSTs are warm) and SAM during this season.

Thus, an increasing body of literature points toward large trends in the SAM being explained not solely by ozone depletion, but also by anthropogenic and natural climate variability, including the variability in the tropical Pacific SSTs. In light of the fact that the ENSO frequency and magnitude have been increasing in the last 50 years (Diaz et al. 2001) and were particularly marked in the 1990s with four El Niño events and two La Niña events (see online at http://www.cpc.ncep.noaa.gov/products/analysis_monitoring/ensostuff/ensoyears.shtml), it is not surprising to see the significant correlations between ENSO and the SAM occurring primarily in the 1990s and only during seasons when ENSO activity is particularly strong.

Although the concept of the tropical SSTs forcing the SAM may be questioned in the SH, similar connections have been established in the NH. Hoerling et al. (2001) using both observations and an atmospheric general circulation model (AGCM) show that the North Atlantic Oscillation (NAO), which is alternatively termed the Arctic Oscillation or Northern Annular Mode (e.g., Thompson and Wallace 2000), is related to tropical SSTs in both the Pacific and Indian Oceans. Their study argues that the observed boreal winter trend in the NAO is intimately linked with the warming in the tropical SSTs, suggesting that the SSTs are forcing the NH extratropical climate. Their earlier work was later updated by more modeling experiments where they further conclude that the tropical Indian Ocean SSTs significantly modulate the NAO (Hurrell et al. 2004; Hoerling et al. 2004).

The exact mechanism controlling the coupling needs further study, and many questions remain unanswered. Examining the role of the meridional circulation across the Southern Hemisphere in relation to the SAM and ENSO variability might help to unlock some of these answers. Additional modeling work, both regionally and globally, can help to demonstrate nonlinear components that lead to the coupling, especially since Hoerling et al. (2004) find that the NAO is strongly modulated by nonlinear atmospheric processes arising from the increasing tropical Indian Ocean SSTs.

6. Summary

Decadal variability of the ENSO teleconnection in the South Pacific has been presented. This decadal variability is observed in many fields including the annual mean MSLP and the 500-hPa geopotential height. Annual mean upper-level wind and MSLP observations are also used to demonstrate the decadal variability and support the spatial representations produced by the ERA-40 reanalysis used in the study. Results in these

annual mean fields indicate a weak teleconnection in the 1980s in a small region in the South Pacific followed by a strong response during the 1990s across nearly the entire South Pacifc and Amundsen–Bellingshausen Seas.

Examining the decadal variability demonstrates that the strong ENSO teleconnection seen in the annual mean plots is accounted for by the teleconnections during SON and DJF. The reduced annual teleconnection during the 1980s is readily explained by the lack of response during SON in the 1980s; during DJF the teleconnection remains strong for both the 1980s and the 1990s although its spatial representation is different. ENSO composites that concentrate on these seasons confirm the decadal variability seen in the correlation plots. Previous studies have not observed the decadal variability as they have averaged over a time interval of more than one decade and only examined connections during austral winter, a season for which no significant correlation was found in the current study.

Through empirical orthogonal function analysis it was found that the patterns correlated with the ENSO and SAM have large loading centers in the South Pacific. As such, the high southern latitude ENSO teleconnection is amplified in the South Pacific during times when the SAM is positively correlated with the SOI, and can be weakened during times of insignificant or negative correlation. The connections between the ENSO and SAM appear only in the seasons when the ENSO forcing is particularly strong, namely, austral spring and summer.

The results presented here, in combination with a growing body of literature, suggest that tropical ENSO activity plays an important role in the forcing of the high southern latitude tropospheric circulation. It is unclear whether the coupling observed here between the high-latitude SH circulation and ENSO is part of natural climate variability or climate change; the quality of the available reanalyses limits the study to roughly the last two decades. However, the associations depicted in the 1990s are the strongest observed during this time period, in agreement with other recent studies (e.g., Bromwich et al. 2004).

Acknowledgments. The authors thank Zhichang Guo for the original design of the program used in calculating the correlations with the SOI, Sheng-Hung Wang for EOF assistance, and Jorge Carrasco for supplying the 500-hPa zonal wind data for Punta Arenas. Comments from two anonymous reviewers helped to clarify and strengthen the manuscript. Discussions with David Thompson are appreciated and also helped to improve the paper. This research was funded in part by NSF Grant OPP-0337948 and UCAR Subcontract SO1-22961.

REFERENCES

Bell, G. D., and M. S. Halpert, 1998: Climate assessment for 1997. *Bull. Amer. Meteor. Soc.,* **79,** S1–S50.

——, and Coauthors, 2000: Climate assessment for 1999. *Bull. Amer. Meteor. Soc.,* **81,** S1–S50.

Bromwich, D. H., and R. L. Fogt, 2004: Strong trends in the skill of the ERA-40 and NCEP–NCAR reanalyses in the high and middle latitudes of the Southern Hemisphere, 1958–2001. *J. Climate,* **17,** 4603–4619.

——, A. N. Rogers, P. Kallberg, R. I. Cullather, J. W. C. White, and K. J. Kreutz, 2000: ECMWF analyses and reanalyses depiction of ENSO signal in Antarctic precipitation. *J. Climate,* **13,** 1406–1420.

——, A. J. Monaghan, and Z. Guo, 2004: Modeling the ENSO modulation of Antarctic climate in the late 1990s with Polar MM5. *J. Climate,* **17,** 109–132.

Cai, W. J., P. H. Whetton, and D. J. Karoly, 2003: The response of the Antarctic Oscillation to increasing and stabilized atmospheric CO_2. *J. Climate,* **16,** 1525–1538.

Cullather, R. I., D. H. Bromwich, and M. L. van Woert, 1996: Interannual variations in Antarctic precipitation related to El Niño–Southern Oscillation. *J. Geophys. Res.,* **101,** 19 109–19 118.

Diaz, H. F., M. P. Hoerling, and J. K. Eischeid, 2001: ENSO variability, teleconnections and climate change. *Int. J. Climatol.,* **21,** 1845–1862.

Genthon, C., and E. Cosme, 2003: Intermittent signature of ENSO in west-Antarctic precipitation. *Geophys. Res. Lett.,* **30,** 2081, doi:10.1029/2003GL018280.

——, G. Krinner, and M. Sacchettini, 2003: Interannual Antarctic tropospheric circulation and precipitation variability. *Climate Dyn.,* **21,** 289–307.

Gillett, N. P., M. R. Allen, and K. D. Williams, 2003: Modelling the atmospheric response to doubled CO_2 and depleted stratospheric ozone using a stratosphere-resolving coupled GCM. *Quart. J. Roy. Meteor. Soc.,* **129,** 947–966.

Gong, D., and S. Wang, 1999: Definition of Antarctic oscillation index. *Geophys. Res. Lett.,* **26,** 459–462.

Guo, Z., D. H. Bromwich, and K. M. Hines, 2004: Modeled Antarctic precipitation. Part II: ENSO modulation over West Antarctica. *J. Climate,* **17,** 448–465.

Harangozo, S. A., 2000: A search for ENSO teleconnections in the West Antarctic Peninsula climate in austral winter. *Int. J. Climatol.,* **20,** 663–679.

Hoerling, M. P., J. W. Hurrell, and T. Xu, 2001: Tropical origins for recent North Atlantic climate change. *Science,* **292,** 90–92.

——, ——, ——, G. T. Bates, and A. S. Phillips, 2004: Twentieth century North Atlantic climate change. Part II: Understanding the effect of Indian Ocean warming. *Climate Dyn.,* **23,** 391–405.

Houseago, R., G. R. McGregor, J. C. King, and S. A. Harangozo, 1998: Climate anomaly wave train patterns linking southern low and high latitudes during South Pacific warm and cold events. *Int. J. Climatol.,* **20,** 793–801.

Hurrell, J. W., M. P. Hoerling, A. S. Phillips, and T. Xu, 2004: Twentieth century North Atlantic climate change. Part I: Assessing determinism. *Climate Dyn.,* **23,** 371–389.

Jones, J. M., and M. Widmann, 2004: Atmospheric science—Early peak in Antarctic oscillation index. *Nature,* **432,** 290–291.

Karoly, D. J., 1989: Southern Hemisphere circulation features associated with El Niño–Southern Oscillation events. *J. Climate,* **2,** 1239–1252.

——, P. Hope, and P. D. Jones, 1996: Decadal variations of the Southern Hemisphere circulation. *Int. J. Climatol.,* **16,** 723–738.

Kiladis, G. N., and K. C. Mo, 1998: Interannual and intraseasonal variability in the Southern Hemisphere. *Meteorology of the Southern Hemisphere,* D. J. Karoly and D. G. Vincent, Eds., Amer. Meteor. Soc., 307–336.

Kwok, R., and J. C. Comiso, 2002: Southern Ocean climate and sea ice anomalies associated with the Southern Oscillation. *J. Climate,* **15,** 487–501.

L'Heureux, M. L., and D. W. J. Thompson, 2006: Observed relationships between the El Niño–Southern Oscillation and the extratropical zonal-mean circulation. *J. Climate,* **19,** 276–287.

Marshall, G. J., 2003: Trends in the Southern Annular Mode from observations and reanalyses. *J. Climate,* **16,** 4134–4143.

——, P. A. Stott, J. Turner, W. M. Connolley, J. C. King, and T. A. Lachlan-Cope, 2004: Causes of exceptional atmospheric circulation changes in the Southern Hemisphere. *Geophys. Res. Lett.,* **31,** L14205, doi:10.1029/2004GL019952.

Mo, K. C., 2000: Relationships between low-frequency variability in the Southern Hemisphere and sea surface temperature anomalies. *J. Climate,* **13,** 3599–3610.

——, and M. Ghil, 1987: Statistics and dynamics of persistent anomalies. *J. Atmos. Sci.,* **44,** 877–901.

——, and W. Higgins, 1998: The Pacific–South American modes and tropical convection during the Southern Hemisphere winter. *Mon. Wea. Rev.,* **126,** 1581–1596.

——, and J. N. Peagle, 2001: The Pacific–South American modes and their downstream effects. *Int. J. Climatol.,* **21,** 1211–1229.

North, G. R., T. L. Bell, R. F. Cahalan, and F. J. Moeng, 1982: Sampling errors in the estimation of empirical orthogonal functions. *Mon. Wea. Rev.,* **110,** 699–706.

Renwick, J. A., 1998: ENSO-related variability in the frequency of South Pacific blocking. *Mon. Wea. Rev.,* **126,** 3117–3123.

——, and M. J. Revell, 1999: Blocking over the South Pacific and Rossby wave propagation. *Mon. Wea. Rev.,* **127,** 2233–2247.

Revell, M. J., J. W. Kidson, and G. N. Kiladis, 2001: Interpreting low-frequency modes of Southern Hemisphere atmospheric variability as the rotational response to divergent forcing. *Mon. Wea. Rev.,* **129,** 2416–2425.

Richman, M. B., 1986: Rotation of principal components. *J. Climatol.,* **6,** 293–335.

Rogers, J. C., and H. van Loon, 1982: Spatial variability of sea level pressure and 500-mb height anomalies over the Southern Hemisphere. *Mon. Wea. Rev.,* **110,** 1375–1392.

Sexton, D. M. H., 2001: The effect of stratospheric ozone depletion on the phase of the Antarctic Oscillation. *Geophys. Res. Lett.,* **28,** 3697–3700.

Silvestri, G. E., and C. S. Vera, 2003: Antarctic Oscillation signal on precipitation anomalies over southeastern South America. *Geophys. Res. Lett.,* **30,** 2115, doi:10.1029/2003GL018277.

Sterl, A., 2004: On the (in)homogeneity of reanalysis products. *J. Climate,* **17,** 3866–3873.

Terray, P., and S. Dominiak, 2005: Indian Ocean sea surface temperatures and El Niño–Southern Oscillation: A new perspective. *J. Climate,* **18,** 1351–1368.

Thompson, D. W., and J. M. Wallace, 2000: Annular modes in the extratropical circulation. Part I: Month-to-month variability. *J. Climate,* **13,** 1000–1016.

——, and S. Solomon, 2002: Interpretation of recent Southern Hemisphere climate change. *Science,* **296,** 895–899.

——, and D. J. Lorenz, 2004: The signature of the annular modes in the tropical troposphere. *J. Climate,* **17,** 4330–4342.

——, J. M. Wallace, and G. C. Hegerl, 2000: Annular modes in the extratropical circulation. Part II: Trends. *J. Climate,* **13,** 1018–1036.

Trenberth, K. E., 1997: The definition of El Niño. *Bull. Amer. Meteor. Soc.,* **78,** 2771–2777.

——, and J. M. Caron, 2000: The Southern Oscillation revisited: Sea level pressures, surface temperatures, and precipitation. *J. Climate,* **13,** 4358–4365.

——, D. P. Stepaniak, and L. Smith, 2005: Interannual variability of patterns of atmospheric mass distribution. *J. Climate,* **18,** 2812–2825.

Turner, J., 2004: Review: The El Niño-Southern Oscillation and Antarctica. *Int. J. Climatol.,* **24,** 1–31.

van Loon, H., and D. J. Shea, 1987: The Southern Oscillation. Part VI: Anomalies of sea level pressure on the Southern Hemisphere and of Pacific sea surface temperature during the development of a warm event. *Mon. Wea. Rev.,* **115,** 370–379.

Wallace, J. M., and D. S. Gutzler, 1981: Teleconnection in the geopotential height field during the Northern Hemisphere winter. *Mon. Wea. Rev.,* **109,** 784–812.

Zhou, T. and R. Yu, 2004: Sea-surface temperature induced variability of the Southern Annular Mode in an atmospheric general circulation model. *Geophys. Res. Lett.,* **31,** L24206, doi:10.1029/2004GL021473.